Integrating Materials and Manufacturing Innovation (2018) 7:52–69
https://doi.org/10.1007/s40192-018-0110-2

THEMATIC SECTION: 4TH WORLD CONGRESS ON INTEGRATED COMPUTATIONAL MATERIALS ENGINEERING

Systems Design Approach to Low-Cost Coinage Materials

Eric A. Lass[1] · Mark R. Stoudt[1] · Carelyn E. Campbell[1]

Received: 13 April 2018 / Accepted: 28 May 2018 / Published online: 20 June 2018

Abstract
A systems approach within an integrated computational materials engineering framework was used to design three new low-cost seamless replacement coinage alloys to reduce the raw material cost of the current US coinage alloys. Maintaining compatibility with current coinage materials required matching the currently used alloy properties of yield strength, work-hardening behavior, electrical conductivity, color, corrosion resistance, and wear resistance. In addition, the designed alloys were required to use current production processes. CALPHAD-based models for electrical conductivity and color were developed to integrate into the system design. Three prototype alloys were designed, produced, and characterized. The design process highlighted the trade-off between minimizing the raw material costs and achieving the desired color properties. Characterization of the three prototype alloys showed good agreement with the design goals.

Keywords CALPHAD · ICME · Materials design · Coinage alloy

Introduction

Desirable coinage materials have long been driven by the supply and cost of the raw materials used to produce coins. In the 1950s and 1960s, the supply of silver decreased, and the cost of then silver coinage materials increased as well as an increased demand for coins. As a result, new coinage materials were sought to replace the silver coinage alloys for the dime and quarter pieces. The US nickel piece has been a copper-nickel alloy (Cu-25Ni mass %, otherwise known as cupronickel) since 1866. However, in 2006, the cost of producing the US nickel exceeded the face value of the coin, as the raw material costs of copper and nickel increased. In 2010, the US Congress established the Coin Modernization, Oversight, and Continuity Act of 2010 (Public Law 111-302 [1]), which authorized the research and development of alternative alloys for coinage materials to reduce current production costs. A comprehensive study of available existing materials and production processes completed in 2012 [2] concluded that while a seamless monolithic replacement alloy produced using current production technologies was preferred, the current existing copper-nickel-based alloys were not suitable seamless replacements for the specific applications using the C73100 alloy (Cu-25Ni mass % alloy). Thus, a systems design approach was employed to design application-specific materials to meet US coinage needs.

A systems design approach, as applied to materials by Olson et al. [3, 4], is based on the well-established materials science paradigm linking processing-structure-properties relations, employing Cohen's reciprocity [5] and integrating the hierarchical structure of materials as defined by Smith [6]. Using this approach within an integrative computational materials engineering (ICME) framework, the specific performance objectives for each application are defined, then the desired microstructural features needed to achieve these properties are determined based on the available processing and property models. The system design approach recognizes that there may be conflicting property objectives that require the system (in this case the material) to be optimized to achieve desired end-material performance and that the designed-material must be robust. That is, small changes in composition and processing will not vary the end-material in-service performance. As such, this is an ideal approach for designing new materials to meet specific coinage application needs.

✉ Eric A. Lass
eric.lass@nist.gov

[1] Materials Science & Engineering Division, Material Measurement Laboratory, U.S. Department of Commerce, National Institute Standards and Technology, 100 Bureau Dr., M/S 8555, Gaithersburg, MD 20899, USA

Within an ICME framework, this work applies a systems design approach to design three new coinage alloys for specific applications. Two of these alloys will be monolithic coinage materials and one will be a cladding material. The specific property needs for each application, as well as some processing constraints, are reviewed. A design approach is outlined using a systems methodology and the required property models are developed and implemented into the design approach. Three prototype alloys are computationally designed and then characterized to determine how well the design objectives are met.

Conceptual Design

Property Objectives

Reducing the cost of the currently used US five-cent piece by 40% with a seamless replacement requires maintaining the following material properties: electrical conductivity, color, yield strength, work hardening behavior, corrosion resistance, and toxicity. Matching the conductivity is essential to maintain compatibility with current vending machine technology. To maintain compatibility, the electromagnetic signature (EMS) of the material must be equal to the EMS of the current alloy. That is, the EMS of a coin is defined as the electrical signal strength of the electromagnetic sensor as the coin passes through the vending machine. Based on this industry definition of the EMS, the coinage material EMS is dependent on the coin thickness and the electrical conductivity of the material. To match the current Cu-Ni alloys in circulation requires a $5.47 \pm 0.10\%$[1] of the International Annealed Copper Standard (IACS, 0.15292 Ω (meter, gram) at 20 °C) and maintaining a density of approximately 8.945 g/cm^3. The color of a material must match the currently used coinage material to maintain esthetic value and public acceptance [1]. The color of the material is defined using the numerical specification of colors with the Commission Internationale de l'Eclairage (CIE) system of colorimetry. The color space is defined by a^* (redness hue), which has a value less than 2.5, and b^* (yellowness), which is less than 10 as measured using spectrophotometery.

The US Mint produces five-cent coins using the following processes: blanking to punch blank coins from coiled strip; upsetting to produce a rim on the coin; and striking to produce the obverse and reverse faces on the coin. These processes require the new materials to have a yield strength less than 200 MPa and corresponding hardness value less than 110 Vickers hardness number (VHN); a tensile elongation to failure exceeding 25%; and a work hardening coefficient equal to that of the current alloy (C71300) values to maintain compatibility with existing equipment.

The behavior of coins in circulation defines the required wear and corrosion resistance properties. Coins must be able to withstand the wear associated with customer use, i.e., rubbing against surfaces and other coins. The coins must also be able to withstand the contact wear associated with a variety of vending machines. The majority of the wear is observed in the thickness of the coin and the loss of detail in the faces. The material must also be corrosion and tarnish resistant as coins are exposed to a variety of environments including human sweat. Coins must also be non-toxic, antifungal, and not leach constituent materials [2]. Current corrosion resistance standards are stated to maintain the color after a 2-hour steam exposure at 100 °C (see previous work [2]).

The ability to easily recycle the material is also a consideration. The current practice is to recycle and reuse all coinage alloys. The lifespan of the typical coin is 30 years after which it is re-melted and minted as new coins.

It should be noted that these property requirements are similar to the requirements specified in the replacement of the silver coinage materials used for the dime and quarter in 1966: availability and price, public acceptance, compatibility with vending machines, impact on the US Mint operations, and anti-counterfeiting [7, 8].

Design Approach

Stossel et al. [2] reviewed several alternate coinage materials and production methods in attempt to reduce the current coinage cost while meeting the desired property objectives. Three alternate Cu alloys were considered: G6 modified by Olin Brass, 669z, and 31157 (both un-plated and nickel plated). While all of these alloys reduce the nickel content and thus offer some raw material cost savings (between 18 and 28%), none of the materials was able to meet the color objectives. In addition, the G6 and 669z alloys required higher annealing temperatures, which would require additional capital investment. A Zn-plated alloy, DuraWhite also reduced the raw material cost, but did not meet the wear requirements. A multi-ply plated steel alloy system was considered but it was not able to match the EMS requirements and could not meet anti-counterfeiting requirements. In addition to requiring higher striking loads and higher annealing temperatures that increased production costs, the Ni-plated steel could not meet the EMS requirement and was not acceptable for plating. A variety of both austenitic and ferritic stainless steel alloys were considered, but these alloys could not match the EMS requirements and required higher striking forces for production, which increased production costs. Schweckandt and Aguirre [9] considered the design of Ni-Co coinage materials and were able to successfully match the conductivity requirements, but not the density. A series of new Cu-based monolithic alloys

[1] The "±" symbol represents one standard deviation.

designed by Song and Hong [10] show potential for meeting the desired property objectives.

Based on this previous work, a system design for a monolithic coinage alloy that meets the property requirements and uses the existing processing constraints from the US Mint was undertaken. The required processing and property requirements are listed in Table 1. To maintain compatibility with US Mint production processes, the processing is limited to casting, rolling, blanking, annealing, anti-tarnish coating, upsetting, and striking. The annealing process that occurs after blanking is limited to 30 min, must occur between 650 and 850 °C, and must be followed by a water quench. Possible alloy systems that could meet these requirements include Al, Cu, Fe, and Zn [2]. Aluminum alloys have good corrosion resistance and electrical conductivity; however, their lower density is problematic in maintaining compatibility with vending machines and for wear resistance. Iron-based and steel alloys offer low-cost solutions, but they have issues with corrosion resistance, cannot match the EMS requirements, have a higher density, and require higher striking forces to produce the coins. A low-cost stainless steel system could be designed; however, the ability to match the required EMS signature is limited. With Zn-based alloys, while corrosion resistant, the oxide film that forms is not particularly attractive and so additional alloying or plating is needed to form an acceptable oxide film on the surface [2]. Cu-based alloys have long been used as coinage materials because of the good corrosion resistance, electrical conductivity, and formability. In addition, the current US production processes are well-suited for processing Cu-based alloys. Therefore, Cu-based alloys were selected as the basis for this design with the goal for reducing the amount of Ni and Cu in the alloy to reduce raw material costs.

A variety of alloying elements can be considered to reduce the amount of Ni in current Cu-based alloys. Song and Hong [10] considered Zn and Fe alloying additions. Breedis [11] considered additions of Zn, Al, Sn, and P to reduce Ni contents and to develop cladding materials for coinage materials. Prinz et al. [12] developed Cu-Al-Ni coinage materials, with Ni contents ranging from 4 to 6 mass % with a small amount of Fe and Mn impurities. While these alloying additions did reduce the material costs, they did not meet the color property objectives. The goal of this design is to use Zn and Mn as the primary alloying additions. This is based on the review of properties of the C77000 Cu-Ni-Zn alloy and the C997xx series of Cu-Ni-Zn-Mn alloys [13, 14]. It is essential that the designed alloy be a single-phase matrix material to avoid the precipitation of the β phase and any ordered phases that could be detrimental to the formability of the alloy. (This requirement will be discussed in greater detail in the "Model Development" section.) Other essential features of the designed alloy are a grain size less than 100 μm (to achieve the desired hardness to ensure successful upsetting and striking of the coins) and the ability to form a stable passive surface film to maintain corrosion and tarnish resistance.

The processing-structure-property relations are summarized in Fig. 1, with the cost being the primary property objective. The essential processing-structure relationships are the ability to produce a single-phase FCC microstructure after casting and avoiding the precipitation of any ordered phases during the annealing process while still producing matrix material with a grain size less 100 μm. The matrix composition and grain size are the primary influences on the yield strength, work hardening rate, and ductility of the material. The ductility is controlled by avoiding the precipitation of ordered phases after annealing. The electrical conductivity is optimized by controlling the Mn concentration and avoiding precipitation of the β phase. The matrix composition, specifically the Ni and Zn contents, and avoidance of precipitates defines the corrosion resistance and the strength of the passivating film formed by the coinage material. The density of the alloy is controlled by maintaining Zn concentration to less than 35 mass percent.

The above systems design approach can also be used to design new low-cost coinage cladding material for use with the 10-cent and 25-cent pieces. For this material, the electrical conductivity property constraint is reduced to approximately 2.0% of the IACS. These processing-structure-property relations and optimization of the conflicting property objectives are integrated into a computational design using several CALPHAD[2]-based composition-dependent models, including thermodynamics, electrical conductivity, color, and cost.

Materials and Experimental Methods

Materials

A variety of alloys were produced as a part of this work ranging from 200 g model alloys to 1 kg prototype alloy compositions. Model binary, ternary, and quaternary alloys in the Cu-Ni-Zn-Mn system were produced in 200 g quantities, while ingots of the prototype alloys were produced in 1 kg size. The initial purities of the pure element starting materials were 0.9995+ Cu, Ni, and Zn, and 0.99+ Mn. Sheets of the commercial alloys C71300 (Cu-25Ni) and C77000 (Cu-18Ni-27Ni)[3] were provided by the US Mint for characterization and comparison with the designed prototype alloys.

[2] CALPHAD originally stood for CALulation for PHAse Diagrams. The method is now used as phase-based modeling for a variety of phase-based material properties.

[3] All alloy compositions provided are given in mass percent unless otherwise noted.

Table 1 Desired design properties for prototypes

Desired property	Alloy Monolithic	Cladding	Low-cost monolithic
Cost	25% reduction	35% reduction	40% reduction
Electrical Conductivity	5.47% ± 0.10 %IACS	2.85% ± 0.10 %IACS	5.35% ± 0.10 %IACS
Color (b*)	7.5	7.5	7.5
Density (g/cm^3)	8.95	8.95	8.95
Yield strength (MPa)	< 200	100–150	< 200
Elongation	> 25%	> 50%	> 25%
Corrosion Resistance	Better than C71300	Better than C71300	Better than C71300
Wear resistance	Better than C71300	Better than C71300	Better than C71300

Materials Processing

All alloys were melted using vacuum-induction melting. To minimize the Zn loss due to evaporation, the overall melting temperature of the ingot was reduced by first melting and re-solidifying the Cu, Ni, and Mn. Once solidified, the Zn was added and the material was then fully melted and stirred by rocking the crucible for a minimum of 2 min. The molten alloys were then pour-cast into Cu-molds. The 200 g ingots were cast into bar-shaped molds with dimensions of 1.3 cm × 2.5 cm × 15 cm high, and the 1-kg ingots were cast into rectangular plate molds with dimensions of about 1.3 cm × 7.6 cm × 10.2 cm high. To ensure a fully dense plate, a graphite hot-top was included on the plate mold (that acted as a reservoir for excess molten alloy), which continued to fill the cavity created via shrinkage during solidification. The excess material left in the hot-top was removed after casting, leaving the plate. The 200 g bar mold did not include such a reservoir. Instead, the top portion of the solidified bar was cut off to a point along the height of the bar where no shrinkage cavity was found in the center of the ingot.

After casting, the bar and plate ingots were rolled to the desired thickness of 1.6 mm through a series of annealing and rolling steps. The ingots were first annealed at a temperature

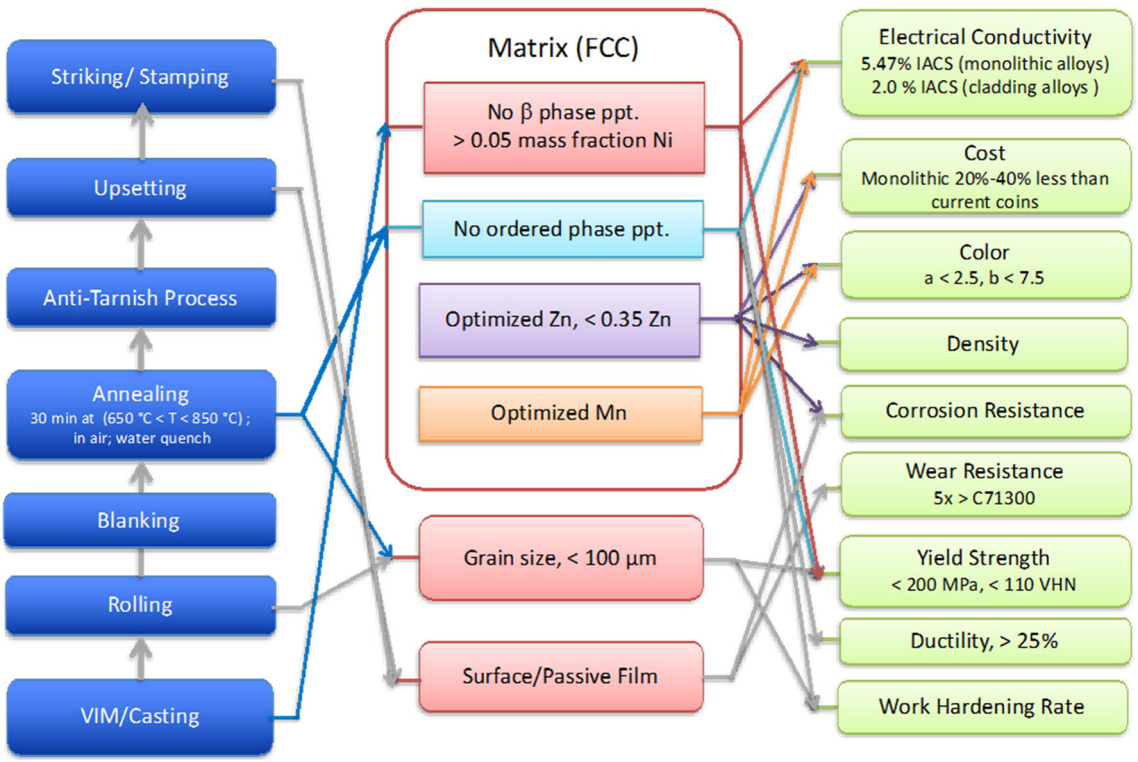

Fig. 1 Schematic illustrating the processing-structure-property relations in the design of low-cost coinage materials. The arrows represent the relations between the processing and structure and the structure and properties. The arrows in gray are not included in this design process

of 750 °C to 800 °C for 30 min in air and then immediately rolled using a Stanat model TA 320[4] rolling mill at a reduction of thickness of 5 to 10% per step. The samples were rolled twice at each reduction step. After a maximum of three reduction steps, the samples were placed back into the furnace and again annealed at 750 to 800 °C, for 15 to 20 min, depending on the size of the ingot. The process of annealing and rolling was repeated until the desired thickness of 1.6 mm was achieved. The alloy sheets were then annealed a final time at 750 to 800 °C for 30 min, followed by a water quench. Finally, the surfaces were cleaned to remove surface scale by a combination of mechanical polishing and chemical etching with an aqueous solution of 20 to 50% acetic acid.

Microstructure Characterization

Several techniques were used to characterize the microstructure including metallography, optical microscopy, x-ray diffraction, and scanning electron microscopy (SEM) with energy dispersive x-ray spectrometry (EDS). Standard metallographic procedures were used to prepare the samples for optical microscopy. The samples were ground to a 1200 grit SiC finish and diamond polished to a 1 μm finish. Carapella's etch (2 mL HCl, 5 g FeCl, 99 mL ethanol) with an immersion for 15 to 20 s was used to reveal the microstructure. X-ray diffraction (XRD) was employed on a limited number of samples to identify the phases present, particularly those that exhibited a two-phase microstructure. SEM was used to evaluate the surface microstructure and identify possible corrosion products produced during exposure to different solutions. EDS measurements were conducted on every sample to determine the alloy composition. A 20 kV accelerating voltage, 0.2 nA beam current, and working distance of 12 mm was used for all EDS measurements. Pure elements were used as standards for quantitative analysis. Several samples were also sent to an independent laboratory for chemical analysis using inductively-coupled plasma (ICP) mass spectroscopy. EDS and ICP composition measurements were found to be consistent with one another.

Mechanical Property Evaluation

Microhardness testing was used to evaluate the strength properties of the alloys after different processing conditions. A micro-Vickers indenter was used with a 200 g load and 10 s dwell time. The mechanical properties of the prototype alloys were evaluated using a servohydraulic tensile frame. Prior to testing, the critical parameters (i.e., gauge length, gauge width, and thickness) were measured for each tensile specimen with a digital micrometer. After centering in the hydraulic grips, the specimen was preloaded to 0.45 kN (100 lbf) and a 12.5 ± 0.15 mm extensometer was attached to center of the gauge section. The specimen was then pulled under constant strain rate conditions at a rate of $\dot{\varepsilon} = 0.015\ \text{min}^{-1}$ until the limit of the extensometer was reached. Then the gauge was removed and the test continued under constant displacement conditions at a rate that achieved a strain rate of $\dot{\varepsilon} = 0.25\ \text{min}^{-1}$ until failure.

Electrochemical Measurements

Prior to evaluating the corrosion behavior of the prototype alloys, coupons of each alloy were polished to a 1 μm diamond finish to remove any mill-scale that may have been present on the surface. Exposure tests were conducted under free corrosion potential (FCP) conditions in two deaerated solutions at room temperature (25 °C). The first solution, 0.5 mol/L sodium sulfate (Na_2SO_4), was used as a reference solution because it generally does not cause pitting in Cu/Ni alloys. The second solution, simulated human sweat, is a composition used by the US Mint to simulate the in-service behavior of a candidate alloy in service. The simulated sweat had the following composition: 40 g sodium chloride (NaCl), 5 g monobasic sodium phosphate ($NaHPO_4$), 4 mL lactic acid ($CH_3CH(OH)CO_2H$), and 4000 mL distilled water (H_2O). A polished coupon was placed in a corrosion cell that was specifically designed to test flat specimens. The area of the sample exposed to the test solution was 0.785 cm^2 for all experiments. Nitrogen gas was bubbled through the solution prior to the test. After 15 min of bubbling, the flow rate was reduced to a slow stream and continued throughout the exposure test. A computer-controlled potentiostat was configured to measure and record the potential with respect to an Ag/AgCl reference electrode at 1-min intervals. Each FCP test was conducted for a period of 24 h.

The FCP is a variable quantity that can be influenced by many factors such as the oxygen concentration in the solution and the active corrosion reactions. While deaerating the solution minimizes the influence of the oxygen on the FCP, it does not eliminate it entirely. For this reason, polarization resistance measurements are a better indicator of the performance for a given alloy in a particular environment. Specimens for these experiments were prepared in the same manner as those used for the FCP measurements. After loading into the corrosion cell, nitrogen gas was slowly bubbled through the solution and the system was allowed to stand for a period of 30 min prior to testing. During this time, the FCP was recorded by the potentiostat. Polarization resistance experiments use a potentiostat to fix the potential at the specimen surface with

[4] Certain commercial entities, equipment, or materials may be identified in this document to describe an experimental procedure or concept adequately. Such identification is not intended to imply recommendation or endorsement by the National Institute of Standards and Technology, nor is it intended to imply that the entities, materials, or equipment are necessarily the best available for the purpose.

respect to a non-polarizable interface, which in this case was an Ag/AgCl reference electrode. The potential is then scanned through a pre-set range. The potential range for these tests started at the lowest potential, − 1.000 V with respect to (wrt) Ag/AgCl reference electrodes, and then stepped at a 5 mV/s rate to the highest potential, which was approximately 0.125 V with respect to Ag/AgCl. The dwell at each potential during the scan was 1 s.

Additional Property Measurements

To best simulate the EMS of the material in service, the electrical conductivity for the different alloys was measured using two different eddy current electrical conductivity meters, a Sigmatest model produced by Foerster, and a Sigma Check produced by Ether NDE. Both meters were calibrated prior to each set of measurements using two conductivity standards provided by the manufacturer, a pure Cu standard (≈ 100% IACS) and an alloy standard with a conductivity of between 5 and 8% IACS. The frequency at which the conductivity is measured influences the measurement as the penetration depth increases with decreasing frequencies. As a result, variations in the sample thickness may influence the conductivity measurement. Consequently, the eddy current electrical conductivity measurements were performed at both 240 and 480 kHz. The color was measured using two spectrophotometers, both supplied by the US Mint. One was a standard production scale spectrophotometer housed at the US Mint's Philadelphia location and one was a portable unit for on-site measurements. Both spectrophotometers are based on the Commission of Illumination (CIE) $L^*a^*b^*$ color space (hereafter referred to as *Lab*), where L^* denotes lightness, and a^* and b^* denote the color-opponent dimensions. In the context of Cu-based coin alloy color, a^* is essentially a measure of "redness" while b^* is a measure of "yellowness." A particular hue can be represented as a vector, i.e., [L^*, a^*, b^*]. Although *Lab* is meant as quantitative measurement of color, color is inherently dependent on material history and measurement conditions. For instance, measurements on C71300 produced b^* values ranging from 5.1 to 8.7, depending on surface preparation, time since the surface was prepared, the spectrophotometer used, and other conditions. The standard for US currency is that $b^* > 10.0$, measured at the production facility in Philadelphia. However, the values measured at the US Mint were found to differ from those measured using a portable, laboratory-based instrument; requiring a change in the target b^* to a value of 7.0 when measured using the portable instrument.

Additional material property testing was conducted by the US Mint, including wear resistance, steam corrosion testing, progressive striking testing, and vending machine testing. The descriptions of these test methods are described in detail in previous reports [2, 13].

Model Development

CALPHAD-based models, which are functional descriptions based on composition and temperature, were developed in the Cu-Ni-Zn-Mn system to predict the phase equilibria, conductivity, color, and cost. Models for the mechanical behavior and corrosion resistance were focused on defining the desirable microstructure elements in the matrix.

Phase Equilibria in the Cu-Ni-Zn-Mn Systems

The binary Cu-Ni phase diagram is relatively simple, containing a single-phase α-FCC solid solution region up to the melting temperatures for all compositions, and is not shown. Phase separation into two FCC phases, one Cu-rich and one Ni-rich, occurs at low temperatures (< 400 °C), but the evolution of this two-phase region is extremely slow, and is of little significance in this study.

Figure 2 presents the binary Cu-Zn phase diagram, calculated using the Thermo-Calc software [15] and the SSOL4 database [16], which illustrates most of the salient phase equilibria features of importance in the quaternary Cu-Ni-Zn-Mn system. A single-phase α-FCC region exists from room temperature to the melting point up to a mass fraction of approximately 35% Zn. Above 35% Zn, the β-BCC and β′-B2 phases become stable, with β forming at temperatures above 450 °C and ordered β′ present below 450 °C. The transition between the two phases is depicted by the dotted line in the figure. Additional phases exist at higher Zn-concentrations, but these are unimportant to the design of Cu-rich alloys based on this system. The binary Ni-Zn phase diagram is similar to that of Cu-Zn, with a large single-phase α-FCC extending

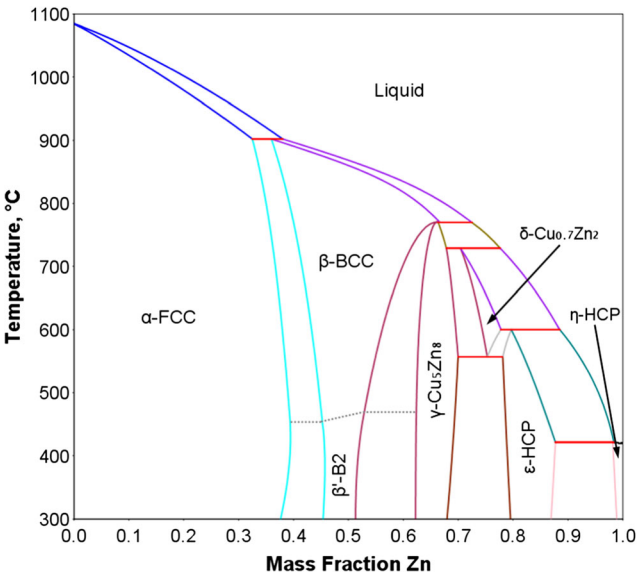

Fig. 2 Binary Cu-Zn phase diagram calculated using the SSOL4 database (the BCC-B2 transition line was added manually)

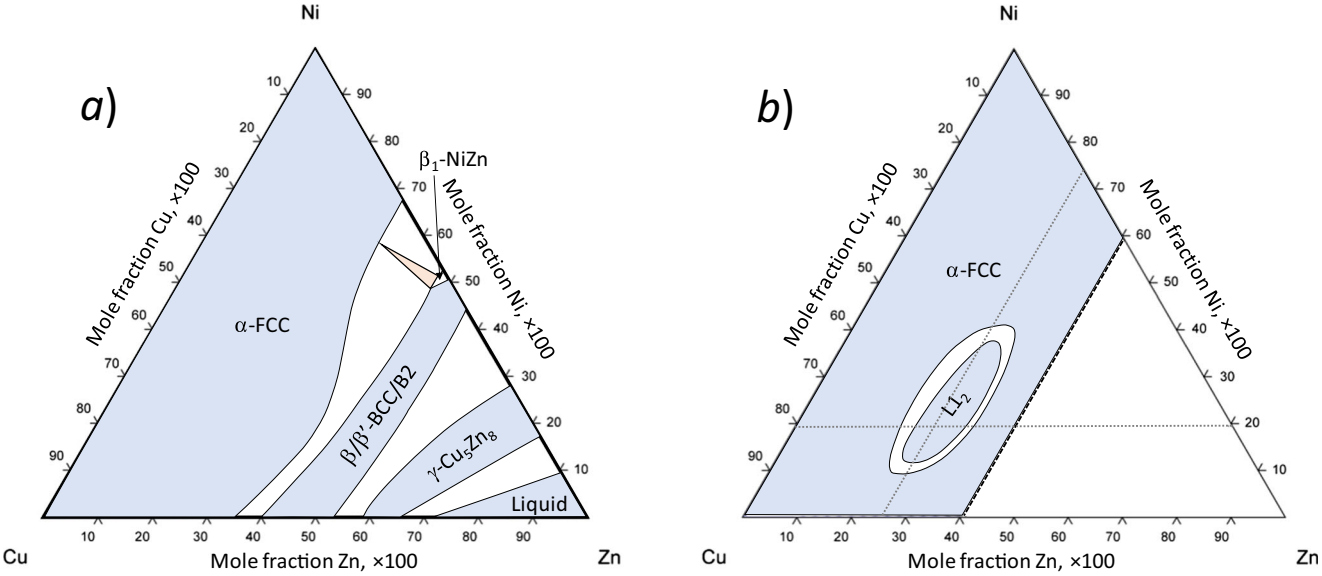

Fig. 3 Isothermal sections of the ternary Cu-Ni-Zn phase diagram at **a** 775 °C [16] and **b** 427 °C [17]. The point of intersection between the two dashed lines in **b** represents the composition of C77000

from room temperature to the melting point for mass fractions of Zn up to approximately 35% and ordered β and β′ phases above 35% Zn.

Two isothermal sections of the ternary Cu-Ni-Zn system, one at 775 °C [17] and one at 427 °C [18], are presented in Fig. 3. As shown in 775 °C isothermal section in Fig. 3a, α-FCC exists over the entire Cu-Ni composition range and up to a mole fraction of Zn of about 35% at temperatures above 500 °C. Below 500 °C, an ordered $L1_2$ structure becomes stable for compositions between 10 and 40% Ni and 20 and 30% Zn mole fraction. At still lower temperatures (not shown), a second ordered phase, $L1_0$, appears near a composition of 20% Ni and 30% Zn. These ordered phases are of significant importance to C77000 and related Cu-Ni-Zn alloys because the ordered phases can have a significant effect on alloy properties, as depicted in Fig. 4. As the cooling rate from the annealing temperature (750 °C) decreases from water quenching (WQ) to furnace cooling (FC), the electrical conductivity decreases from about 5.7 to 5.1% IACS, while the Vickers microhardness increases from < 100 VHN to almost 120 VHN. Therefore, how the material is cooled after annealing is a critical step in the processing sequence to ensure the desired properties. The production facilities for coin manufacturing in the United States use water quenching following the annealing step. For this reason, the alloys were designed so that the electrical conductivity and microhardness exhibited the correct properties after water quenching. With these design criteria, no further consideration was given to the effects of ordering and quenching on material properties.

Two thermodynamic assessments of ternary Cu-Ni-Zn have been published, one by Jiang et al. [19] and one by Miettinen [20]. The Miettinen description is limited to temperatures of 600 °C and above, and therefore, does not contain descriptions for the ordered $L1_2$ and $L1_0$ phases that occur at lower temperature. However, Miettinen has also performed thermodynamic assessments for ternary Cu-Mn-Ni [21] and Cu-Mn-Zn [22] using the same unary and binary subsystem assessments, providing a self-consistent description of the thermodynamics and phase equilibria in the quaternary Cu-Ni-Zn-Mn system of interest. Therefore, Miettinen's thermodynamic descriptions were used in the present alloy design process. As stated above, the potential effects of ordering at intermediate temperatures are mitigated by designing the alloy around a water quenching from the annealing temperature.

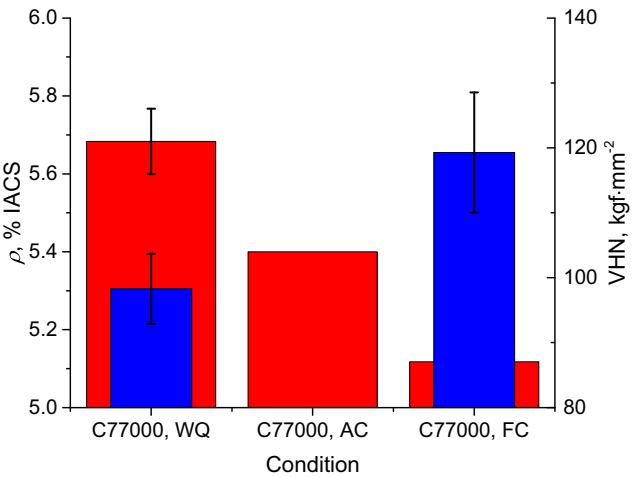

Fig. 4 Effect of cooling rate (i.e., ordering) from an annealing temperature of 750 °C on the electrical conductivity (wide bar) and Vickers microhardness (narrow bar) of commercial C77000 (*WQ* water quenched, *AC* air cooled, *FC* furnace cooled). The uncertainty of *r* for the FC sample (obscured) is ± 0.05% IACS (where ± equals one standard deviation). No microhardness or uncertainty measurement was reported or the AC condition

Figure 5 presents an isothermal section at 500 °C of the quaternary system, calculated using the combined thermodynamic assessments of Miettinen, for a constant mass fraction of Cu of 55%. A phase boundary exists between two-phase FCC + BCC and single-phase FCC in the Cu-Zn-rich corner (lower-left). The single-phase FCC region exists for compositions above a Ni mass fraction of 3%. A minimum mass fraction of 5% Ni was chosen to ensure any designed alloy consisted of a single-phase FCC microstructure.

Electrical Conductivity Modeling

Campbell et al. [23] proposed a CALPHAD approach to modeling electrical conductivity, which is the inverse of the electrical resistivity following the approach demonstrated by Nordheim [24] and Terada [25], who expressed the electrical resistivity in a metallic binary solid solution the sum of the pure component contributions and a mixing term. Following this approach, a CALPHAD-type model describing the composition dependence of the room temperature electrical resistivity was constructed for the quaternary Cu-Ni-Zn-Mn system. For a binary A-B system, the electrical resistivity of a phase ϕ, ${}^{\Phi}\rho$, is described by the equation

$$ {}^{\Phi}\rho = x_A {}^{\phi}\rho^{o}_{A} + x_B {}^{\Phi}\rho^{o}_{B} + x_A x_B \sum_i (x_A - x_B)^i {}^{\Phi}\rho^{i}_{AB} \quad (1) $$

where x_J is the mole fraction of species J, ${}^{\Phi}\rho^{o}_{J}$ is the electrical resistivity of component J in the form of phase ϕ, and ${}^{\Phi}\rho^{i}_{AB}$ are the ith-order interaction parameters of A and B in the form of phase ϕ that describe the behavior of the electrical resistivity of an A-B solution. The ${}^{\Phi}\rho^{o}_{J}$ and ${}^{\Phi}\rho^{i}_{AB}$ may have a temperature-dependent component, but, as mentioned above, only room temperature electrical resistivity is considered in this work. As FCC is the only phase considered in the current electrical resistivity model, ϕ has been omitted from the notation in the remainder of this work.

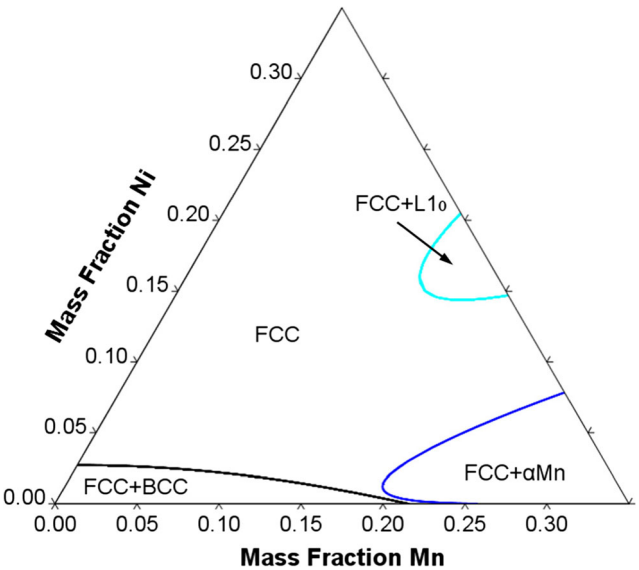

Fig. 5 Calculated isothermal section of the quaternary Cu-Ni-Zn-Mn phase diagram at 500 °C for a constant mass fraction of Cu of 55%

The electrical resistivity descriptions for three binary subsystems are then combined to construct a ternary description. Any available ternary data can be used to determine ternary mixing terms, described by

$$ \rho_{ABC} = x_A x_B x_C \sum_{i=0}^{2} x_i \rho^{i}_{ABC} \quad (2) $$

where the x_i in the summation are x_A, x_B, and x_C for i equal to 0, 1, and 2, respectively, and the ρ^{i}_{ABC} are the ternary interaction parameters for each term in the summation. In some cases, a single ternary interaction parameter is specified, in which case all ρ^{i}_{ABC} are equal and the summation in Eq. (2) collapses to ρ^{0}_{ABC}. Finally, a multi-component description is built from the ternary subsystems. Mixing interactions beyond ternary are typically negligible and are not considered in this work.

Table 2 lists the room temperature electrical resistivity of the pure elements (unary). A value for Zn in the FCC crystal structure was not available, so the electrical resistivity of the HCP phase was used. Most of the composition-dependent electrical resistivity data for the binary alloys were taken from the *Handbook of Electrical Resistivities of Binary Metallic Alloys* [26]. Reported results for selected Cu-based commercial binary and ternary alloys were also included, along with experimental measurements made as a part of this work. All of

Table 2 Optimized parameters used to describe the composition dependence of the electrical resistivity of the FCC phase in the quaternary Cu-Ni-Zn-Mn system

System	ρ^{o}_{J} ($\mu\Omega$ cm)	$\rho^{0}_{AB(C)}$	$\rho^{1}_{AB(C)}$	$\rho^{2}_{AB(C)}$
Cu	1.72			
Mn (fcc)	23			
Ni	6.58			
Zn (hcp)	5.45			
Cu-Mn		653.23	− 394.72	
Cu-Ni		179.12	− 10.61	− 59.33
Cu-Zn		17.27	8.27	
Mn-Ni		419.94	192.11	
Mn-Zn		300		
Ni-Zn		20	5	
Cu-Mn-Ni		− 258.34		
Cu-Mn-Zn		26.95		
Cu-Ni-Zn		− 108.43	937.97	435.36

The electrical resistivity of HCP Zn was used because no value for FCC Zn could be found

the experimental data considered were measured at room temperature and in the annealed condition, except for a few values reported for commercial alloys where no processing history was given. (The data used to develop this composition-dependent conductivity model and other phase-based models is available in supplement data reference [14].) Table 2 lists the assessed parameters for the six binary and three Cu-containing ternary systems that comprise the quaternary Cu-Ni-Zn-Mn system. No experimental data were available for the two binary alloys, Ni-Zn and Mn-Zn. The binary Ni-Zn phase diagram is similar to that of Cu-Zn, so it is assumed that the electrical conductivity also behaves similarly, and the ${}^{\phi}\rho_{NiZn}^{i}$ were chosen to reflect this similarity. The electrical resistivity of Mn-Zn is expected to behave like the two other Mn-containing systems and is described by a single interaction parameter ${}^{\phi}\rho_{MnNi}^{0}$. Figure 6 presents the comparison between calculated electrical resistivity and experiment for the six binary alloy systems. There is good agreement between experiment and model in all cases where experimental data is available.

Figure 7 presents the electrical conductivity as a function of composition in the Cu-Ni-Zn and the Cu-Ni-Zn-Mn systems. Figure 7a presents the calculated electrical conductivity (in % IACS) for ternary Cu-Ni-Zn in the Cu-rich corner of the composition space. The iso-conductivity contour lines are nearly parallel to the Zn-axis, indicating that Zn-content has little effect on conductivity. The calculated conductivity of Cu-18Ni-27Zn (commercial ternary C77000) is 5.75% IACS, which is slightly higher than the reported 5.5 to 5.7% IACS because the commercial alloy contains minor alloys elements and impurities (specifically C77000 contains < 0.3% Mn, which if included in the model reduces the calculated electrical conductivity of C77000 to 5.53% IACS). Figure 7b shows a plot of calculated electrical conductivity in quaternary Cu-Ni-Zn-Mn as a function of Ni- and Mn-content for a constant Cu-concentration of 55%. The electrical conductivity drops off rapidly as Ni- and Mn-content increases. The iso-conductivity lines are closer to parallel with the Ni-axis, indicating that Mn is more potent at reducing electrical conductivity than Ni by roughly a factor of two.

Color Modeling

As maintaining the same color is a requirement for a seamless replacement alloy, a composition-dependent color model was employed. The first composition-dependent color model was presented by Lahiri et al. [27] for the Cu-Mn-Zn system. Lahiri et al. determined the white, yellow, or red values for various ternary alloys in the system and then plotted constant color lines. German et al. [28] expanded this approach to dental alloys focusing on the Ag-Au-Cu system. This work expands this approach by using a CALPHAD approach to define

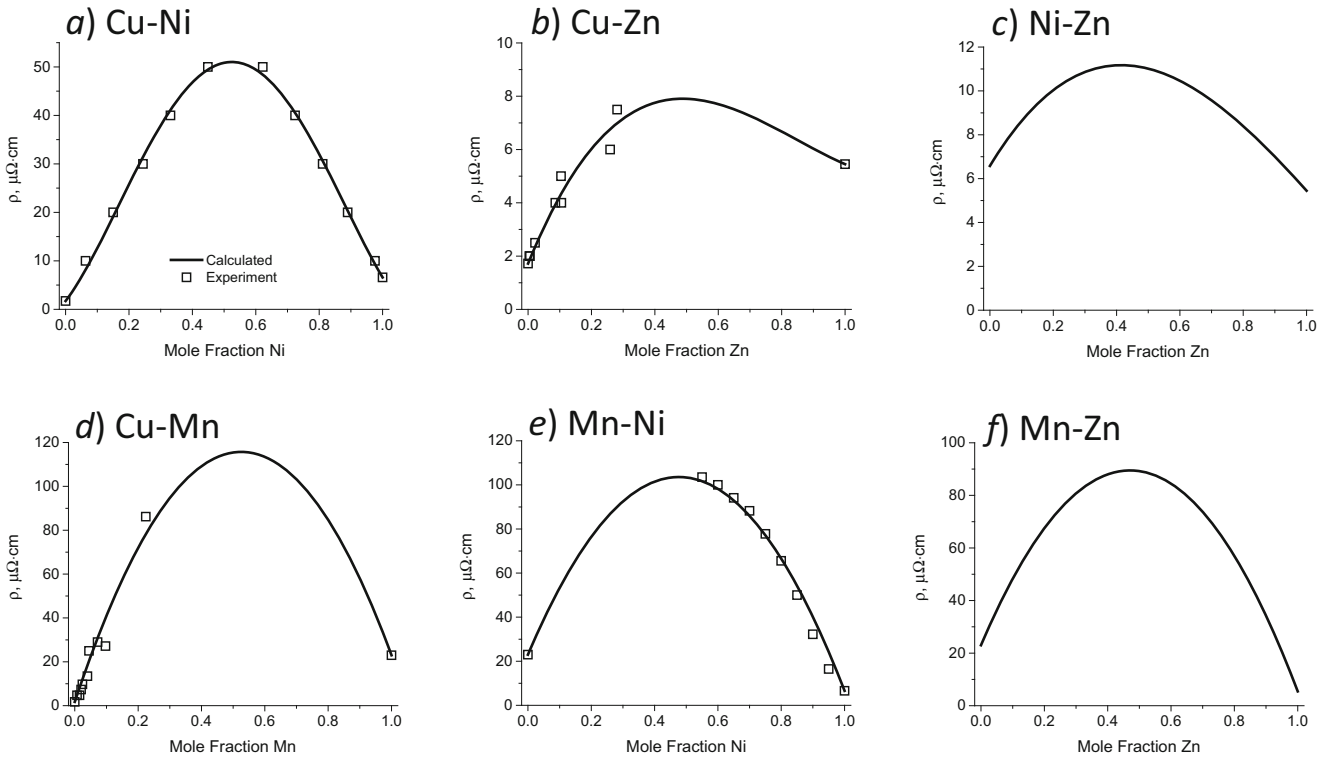

Fig. 6 Composition-dependent electrical resistivity behavior calculated compared to the experimental data for the six binary subsystems of the Cu-Ni-Zn-Mn system

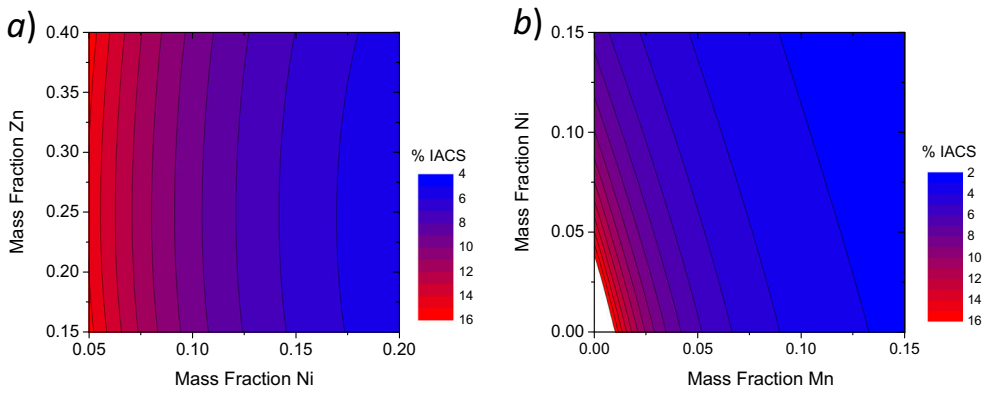

Fig. 7 Composition-dependent model of electrical conductivity constructed for the **a** ternary Cu-Ni-Zn system and **b** quaternary Cu-Ni-Mn-Zn system for a constant mass fraction of Cu of 0.55

the composition dependence of the color. All other color data was determined via experimental investigation in the present study. A set of five test alloys with compositions given by Cu-5Ni-(40-*x*)Zn-*x*Mn (where $x = 5$, 10, 15, 20, and 25) were produced to provide an initial set of color (as well as electrical conductivity and Vickers microhardness) data for quaternary Cu-Ni-Zn-Mn alloys. Figure 8 presents the measured electrical conductivity, Vickers microhardness, and b^* color vector for these five alloys in the annealed and water-quenched condition. The b^* color vector of the 5Mn alloy is quite high, ≈ 11, and continuously decreases with increasing Mn-content. The electrical conductivity also decreases with increasing Mn-content while the Vickers microhardness shows the opposite trend. These experimental measurements, along with additional data points collected during the course of the early design process, were used to construct a composition-dependent

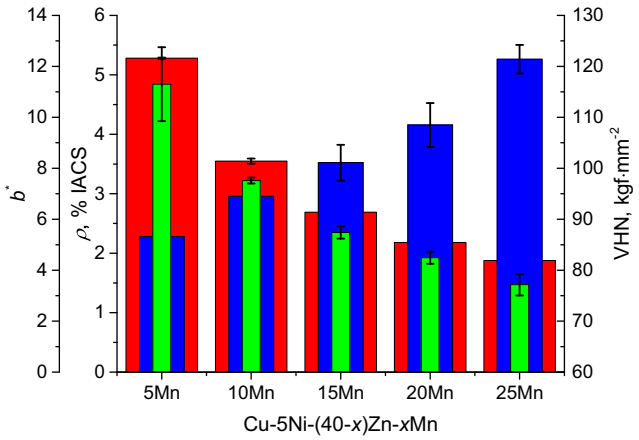

Fig. 8 Electrical conductivity (widest bar), Vickers microhardess (medium-width bar), and b^* color vector (narrow bar) of the five test alloys with compositions given by $Cu_{55}Ni_5Zn_{40-x}Mn_x$, produced for calibrating the electrical conductivity model of the quaternary Cu-Ni-Mn-Zn system. The obscured uncertainty bars are similar to the visible ones

description of the b^* color vector. The finalized composition-dependent color model is given by the following equation

$$\begin{aligned} b^* = {} & A + Bw_{\mathrm{Mn}}w_{\mathrm{Ni}} + Cw_{\mathrm{Mn}}w_{\mathrm{Zn}} + Dw_{\mathrm{Ni}}w_{\mathrm{Zn}} \\ & + Ew_{\mathrm{Mn}}w_{\mathrm{Ni}}w_{\mathrm{Zn}} + Fw_{\mathrm{Mn}}{}^2w_{\mathrm{Ni}} + Gw_{\mathrm{Mn}}{}^2w_{\mathrm{Zn}} \\ & + Hw_{\mathrm{Mn}}w_{\mathrm{Ni}}{}^2 + Iw_{\mathrm{Ni}}{}^2w_{\mathrm{Zn}} + Jw_{\mathrm{Mn}}w_{\mathrm{Zn}}{}^2 \\ & + Kw_{\mathrm{Ni}}w_{\mathrm{Zn}}{}^2 \end{aligned} \tag{3}$$

where w_J is the mass fraction of component J, and A through K are fitting parameters. Several additional terms were considered, including the first- and second-order terms in w_J and w_J^2, which produced slightly more accurate b^* values for the intermediate compositions. However, these terms produced unrealistic values for compositions outside of the experimentally investigated composition space and were excluded from the final model.

Table 3 presents the assessed fitting parameters for b^* in the Cu-Ni-Zn-Mn system. Figure 9 presents the predicted b^* value for ternary Cu-Ni-Zn in the Cu-rich corner of the composition space and in quaternary Cu-Ni-Zn-Mn as a function of Ni- and Mn-content for a constant Cu-concentration of 55%. In the ternary Cu-Ni-Zn alloy, Fig. 9a, b behaves similarly to the electrical conductivity, in that it is most dependent on Ni-concentration and decreases with increasing Ni-content. In the quaternary alloy, Fig. 9b, Ni is predicted to be more effective than Mn at decreasing b^*. For example, the b^* for an alloy containing 10% Ni approaches 10.0 as Mn-content goes to zero, whereas the b^* for an alloy containing 10% Mn is closer to 11.5 as Ni-content vanishes. Note that the predicted color for alloys with high concentrations of both Ni and Mn, shown in the upper right-hand corner of Fig. 9b, are not accurate because no experimental data are available for this composition range. However, alloy compositions were limited to Mn + Ni concentrations of roughly ≤ 20%, so this composition range was not used in the design process.

Table 3 Assessed parameters for the color model used for alloy design, described by Eq. (4)

A	B	C	D	E	F	G	H	I	J	K
15.0	− 531	− 181	− 331	− 554	− 1530	− 319	− 337	5420	33.6	653

Cost Modeling

A simple description for the materials cost of the alloy was included in the design optimization process. The price per kilogram of the raw elements when the project began in 2014 were used to compute alloy cost, and is given by the equation

$$\text{cost}\ (/\text{kg}) = 7.8w_{\text{Cu}} + 2.3w_{\text{Mn}} + 14.5w_{\text{Ni}} + 2.1w_{\text{Zn}} \qquad (4)$$

The cost of C71300 is $9.46 per kg. Ni has the largest influence on the overall cost, while Cu has the second largest impact on the alloy cost. The primary design objective was therefore to replace as much Ni as possible with Mn and Cu with Zn, while maintaining the desired material properties. A materials cost saving of 20 to 25% or more was desired, without requiring changes to the coin manufacturing operation.

Other Properties

Previous work to quantify the corrosion mechanisms associated with Cu-base alloys found the corrosion behavior highly dependent on the solution in which the behavior is characterized [29–32]. The most recent work by Porcayo-Calderon [32] showed that in Cu-Ni-Zn alloys, the corrosion performance is function of the Zn/Ni ratio, with an increasing ratio improving the corrosion performance. Prior research by US Mint [2, 13] identified the C77000 alloy, which has a Zn/Ni ratio of 27/18 ratio, as having acceptable corrosion-wear resistance behavior based on steam testing. This design work takes a simplified approach to modeling the corrosion behavior by just maintaining a Zn/Ni of 27/18 or higher. Similarly, acceptable wear properties were assumed to be achieved by avoiding precipitation of unwanted phases, achieving an approximate 100 μm grain size and a hardness of 100 VHN would be sufficient. This is based on reviewing previous work by US Mint [13] and Stossel [2].

Design of Prototypes

The key elements of the overall design strategy for all the prototype designs is outlined in Fig. 10. The initial Cu, Mn, and Ni content are determined using Eq. 3 to obtain the desired color with single-phase matrix structure after water quenching from the annealing process. To obtain a single-phase matrix requires that the Zn content remain below 35 mass % based on Fig. 3a and that the Ni composition to be at least 5 mass % to allow the later additions of Mn without forming the β brass phase (see Fig. 5). The restriction on Ni-content was further raised to a minimum of 6 mass % after a small fraction of β brass was observed in the microstructure of test alloy C99E, which are observed in Fig. 12a as dark precipitates along grain boundaries. Figure 9 shows the trade-off between Mn and Ni that defines the color of material. Next, the Ni and Mn contents are optimized to obtain the desired electrical conductivity using the CALPHAD model in Eqs. 1 and 2. Then the cost is minimized by the replacement of Cu with Zn using Eq. 4. Finally, the overall composition is optimized to ensure the key design objectives, color, and electrical

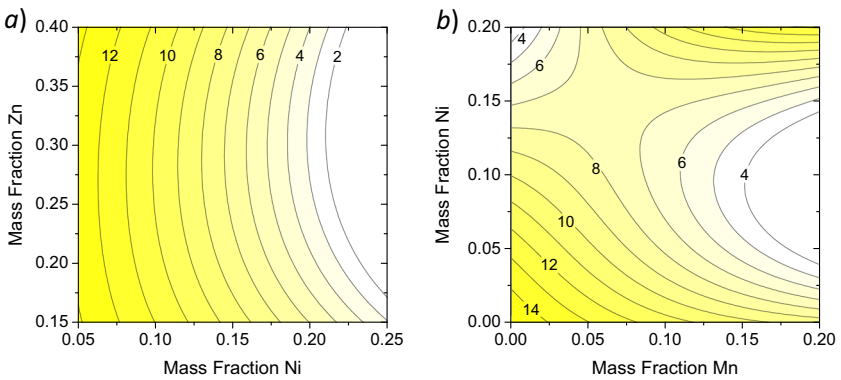

Fig. 9 Color model used to predict b^* color vector ("yellowness") as a function of composition in **a** ternary Cu-Ni-Zn and **b** quaternary Cu-Ni-Zn-Mn for constant mass fraction of Zn of 25%

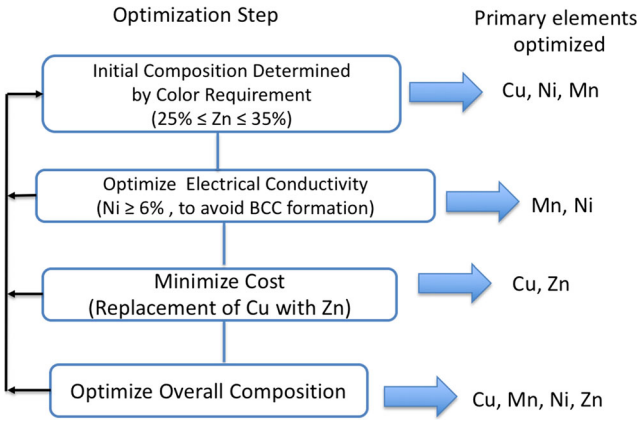

Fig. 10 Flowchart for key design calculation. Right side indicates the primary elements that are optimized during each design step

conductivity are achieved at minimum cost. The design process is repeated until an optimal composition is determined.

Alloy #1: C77000 Modification

The first designed prototype alloy is a modification of the commercial alloy C77000, altered to match the electrical conductivity of C71300, 5.49 ± 0.18% IACS, to within 0.2% IACS when water-quenched from the annealing temperature. As mentioned above, C77000 is a commercial ternary alloy with the composition Cu-18Ni-27Zn that contains minor alloys elements and impurities, specifically up to 0.5% Mn and up to 0.25% Fe. The reported electrical conductivity of C77000 is 5.5 to 5.7% IACS, but no processing history is reported with these values. From Fig. 4, the electrical conductivity of water-quenched C77000 is 5.68 ± 0.12% IACS. Using the electrical conductivity model presented in Eqs. 1 and 2, the calculated electrical conductivity of ternary Cu-18Ni-27Zn is 5.73% IACS (the uncertainty of the model is estimated to be about ± 0.20% IACS), while that of quaternary Cu-18Ni-27Zn-0.3Mn is 5.53% IACS. These results indicate that Mn-content must be considered even for concentrations < 1%.

For this design, the color properties are defined by the initial C77000 matrix composition: Cu-18Ni-27Zn. The Mn is added to the initial matrix composition to meet the electrical conductivity requirement: 5.49 ± 0.18% IACS. Additional optimization using the electrical conductivity model predicts that replacing 1% Zn with Ni reduced the electrical conductivity by ≈ 0.2% IACS, to 5.31% IACS. After one iteration of the design process, composition of the C77000-modified prototype alloy is Cu-19Ni-26Zn-0.3Mn, which is dubbed C77D [33].

Alloy #2: C99-Series Cladding Alloy

The second prototype alloy composition developed is for a proposed cladding application for multilayer coinage. The electrical conductivity requirement is lower than that of C71300, between 2 and 3% IACS, while retaining all the remaining requirements for the monolithic alloy. The color is required to be white, as defined by the b^* being < 7. The yield strength of the material should remain between (100 and 150 MPa) with a 50% ductility. The cost of the raw materials must be reduced by 25%. The reduction in electrical conductivity allows the more expensive Cu core to be thinner (with a thicker cladding layer) for a coin with the same total thickness as the presently used nickel, while maintaining the same eddy current electrical signature. The cost for the multilayered coin is reduced in two ways: (1) a less expensive cladding layer; and (2) less Cu is required for the core. With these assumptions, the Ni content is reduced to 6 mass % and the Mn and Zn contents are adjusted to meet the cladding requirements. Figure 8 shows the trade-offs among the electrical conductivity, color, and hardness properties as the Mn and Zn contents are varied. The electrical conductivity increases with decreasing Mn additions, while the hardness increases with increasing Mn additions. The desired color is optimized with a Mn content between (10 and 15) mass %. Based on these conflicting objectives, the Mn and Zn contents are set at 12.5 Mn mass % and 25 Zn mass %, and Ni content was kept at the minimum of 6 mass % to minimize cost. After this optimization, a new cladding alloy is proposed with a composition of Cu-6Ni-25Zn-12.5Mn [34].

Alloy #3: C99-Series Monolithic Alloy

The third prototype alloy design is a monolithic alloy with the lowest possible materials cost that possesses an electrical conductivity of (5.35 ± 0.2) % IACS (reduced to account for the lower density and the slightly thicker coin design compared to C73100 to maintain an equivalent EMS and piece mass), while maintaining the hardness, work hardening, wear resistance, and corrosion behavior of C73100. The initial design matrix of Cu-5Ni-35Zn-5Mn was selected to maximize the reduction in the raw materials cost (Eq. 4), while maintaining a single-phase matrix microstructure after annealing. The electrical conductivity model was used to determine constant bands of electrical conductivity as functions of the Ni and Mn content. These results were then superimposed on the color model results. Figure 11 presents a cross-plot of the design constraints for the electrical conductivity and color for this design. For a constant mass fraction of 55% Cu, the b^* color vector was plotted as function of Ni and Mn compositions and (5.32 ± 0.2) % IACS contour bands are overlaid on the color contours. The initial optimized composition identified, labeled C99G in Fig. 11, meets all the initial requirements. After experimental characterization of C99G, a modification to the color requirement was made reducing the allowable b^* to less than 7.5. Further optimization using the new color allowable reveals that an alloy meeting the electrical conductivity and a $b^* \leq 7.5$ will have at least 13 to 14% Ni

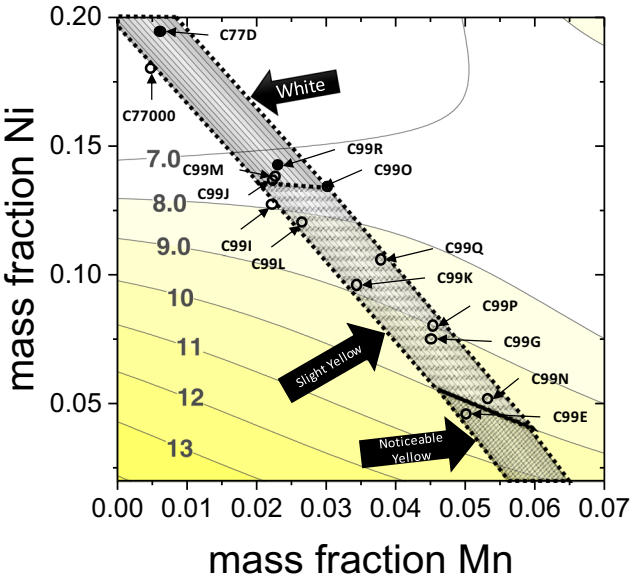

Fig. 11 Cross plot of b^* color vector (numbered contour lines) and electrical conductivity (grayscale band with center corresponding to 5.35% IACS and the gray bands extending ± 0.25% IACS from that value) for a constant mass fraction of 26% Zn

and no more than about 3% Mn. This figure shows that to maintain the required conductivity, there is a direct tradeoff between decreasing cost and color as a result of varying the Ni-content. Several additional data points for model alloys produced during this work [14] to further demonstrate the direct trade-off between alloy cost and color are included in Fig. 11. The optimized prototype alloy composition is identified to be Cu-14Ni-28.5Zn-2.5Mn [35].

Prototype Characterization

Vacuum induction melting was used to make four 1.5 kg ingots of designed prototypes. These prototypes were hot rolled to the desired 1.63 mm thickness to be compatible with the US Mint blanking and stamping processes. The average thickness of the rolled ingots was 1.63 ± 0.051 mm. Following hot rolling, the ingots were annealed, and water quenched. A portion of the annealed sheets, totaling 2 kg in mass, were sent to the US Mint. The remaining material from each design prototype was characterized to determine how well the alloys meet the design objectives. The compositions of each ingot were measured using EDS after rolling into sheet and found to be consistent with one another and with the target composition to within about 2% Zn, 0.5% Ni, and 0.1% Mn. Optical microscopy confirmed a single-phase FCC microstructure for all three prototype compositions as seen in Fig. 12b with average grain sizes < 100 μm. The measured compositions are given in Table 4. XRD measurements revealed that the FCC α phase was the only phase present in all the prototype alloys. One design model alloy, Cu-5Ni-35Zn-5Mn, contained the β phase, in addition to the FCC phase. After confirming that the desired FCC microstructure was obtained, the electrical conductivity and color were measured and are also reported in Table 4.

Mechanical Properties

The mechanical properties for each design prototype were characterized using several methods. The Vickers hardness for each alloy is reported in Table 4. Figure 13 compares the representative true tensile stress-strain behavior of the C77D, C99R, and C99H to the commercial C71300, and the C77000. Figure 13a shows that both the C77D and the C77000 are significantly stronger and more ductile than the binary C71300. Similar mechanical properties were expected for C77D and C77000 as the compositions are similar. The slightly lower yield strength, ultimate tensile strength, and slightly higher ductility of C77D compared to the C77000 are most likely due to the presence of tramp impurities in the C77000 alloy. Figure 13b shows that C99R is stronger and more ductile than the C71300, although the yield strength is nearer to that of C71300. The results from the mechanical property analyses for the prototypes and the commercial alloys are summarized in Table 5. The properties K and η are the work hardening coefficient and exponent, respectively, which are related to the true stress-strain curve by the following equation:

$$\sigma = K\varepsilon^{\eta} \tag{5}$$

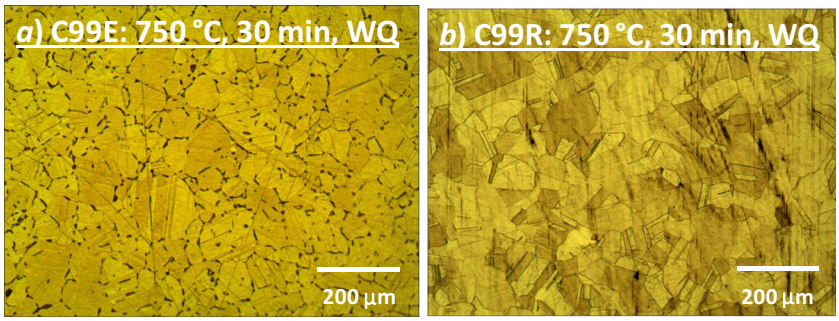

Fig. 12 Microstructure of C99E and C99R after annealing 750 °C for 30 min followed by a water quench. The dark precipitates along the grain boundaries of C99E are β-phase

Table 4 Composition and properties of alloy prototypes compared to the current commercial alloy in use and commercial C77000

Alloy	C71300	C77000	C77D [32]	C99H [33]	C99R [34]
Cu, %	Bal.	53.5 to 56.5	Bal.	Bal.	Bal.
Ni, %	23.5 to 26.5	16.5 to 19.5	19.3 ± 0.5	6.2 ± 0.2	14.4 ± 0.4
Zn, %	< 1.0	Bal.	26.2 ± 0.6	25.1 ± 0.6	28.1 ± 0.5
Mn, %	< 1.0	< 0.5	0.3 ± 0.1	12.6 ± 0.1	2.3 ± 0.1
Other, %	Fe: < 0.20	Fe: < 0.25	N/A	N/A	N/A
σ, % IACS	5.49 ± 0.18	5.5 to 5.7	5.44 ± 0.36	2.83 ± 0.15	5.37 ± 0.12
VHN, kgf·mm^{-2}	102 ± 22	108 ± 5	105 ± 7	94 ± 5	93 ± 6
b^*	5.6 ± 0.6	5.5 ± 0.2	< 7.0	5.2 ± 0.2	7.4 ± 0.5
Potential[a] Na_2S0_4 (V)	− 0.03	− 0.03	− 0.18	− 0.2	− 15
Sweat solution (V)	− 0.185	− 0.215	− 0.215	− 0.26	− 0.235
Cost compared to C71300	100%	80%	80%	65%	75%

[a] Potential measured after 24 h in stated solution

On a log plot, these values are the intercept and slope of the true stress strain curve respectively. The K and η values were determined over two strain regions: from 0.01 to 0.1 and from 0.1 to 0.15. The former range defines the work hardening just beyond the yield, and is of particular interest to coin stamping processes. The second range denotes a region where the plastic flow (work hardening rate) has stabilized. Note the initial work hardening of C77D, C99R, and C77000 are lower than C71300, which suggests that both these alloys may flow more easily than C71300 during the coin stamping process. The yield strength and work hardening behavior of prototype alloy C99H are even lower than that for C99R. This is slightly surprising since the alloying element content of C99H is greater than that of C99R. However, if only the Mn + Ni content is considered, the yield strength (and work hardening parameters) scale with this value for all three alloys. That is, C77D with an Mn + Ni of 19.6% is the "strongest" while C99H with an Mn + Ni of 16.7 is the "weakest," and C99R is in between the two. This suggests that the Zn-content plays only a small role in the solid solution strengthening behavior of these alloys.

Electrochemical Behavior

The electrochemical behavior of the three prototypes was evaluated by measuring the free corrosion potential (FCP) and polarization curves in both a deaerated Na_2SO_4 solution

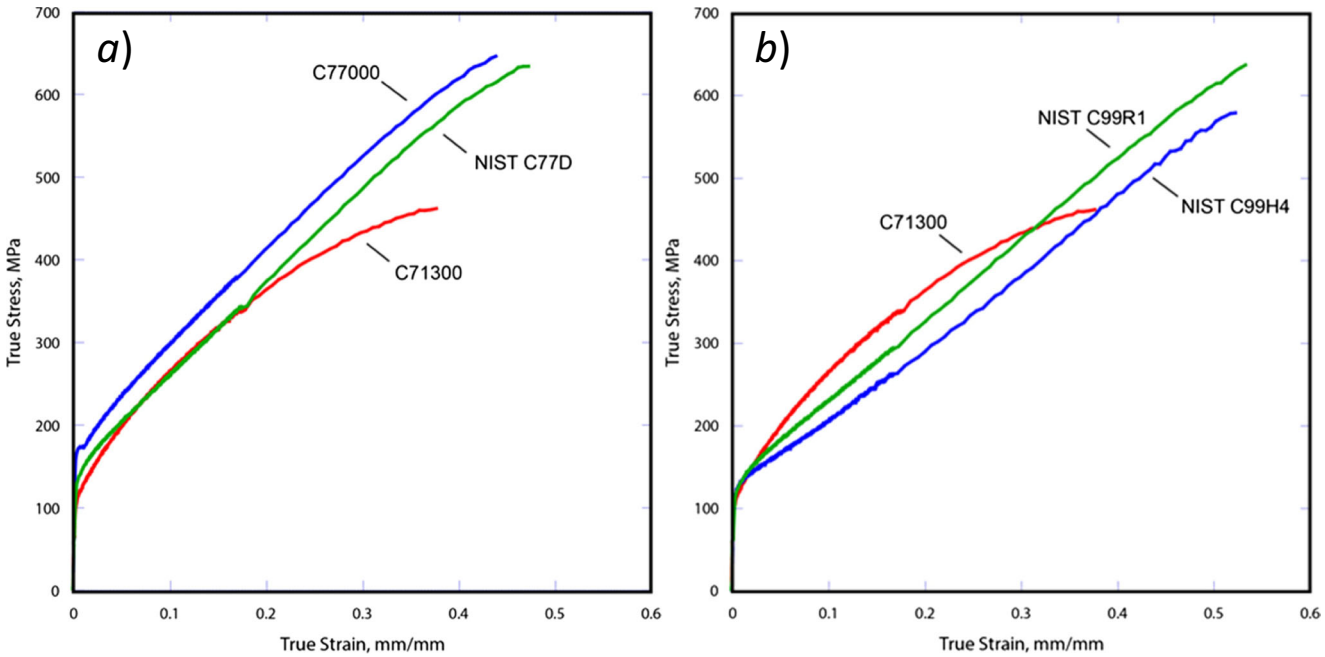

Fig. 13 Representative tensile stress strain curves for **a** commercial C77000 and prototype alloy C77D and **b** prototype alloys C99H and C99R, compared to commercial alloy C71300, which the alloys are designed to replace

Table 5 Mechanical properties of the three prototype alloys developed in the present work compared to commercial alloys C77000 and C71300

Alloy	C71300	C77000	C77D	C99R	C99H
σ_y, MPa	113 ± 8	164 ± 2	129 ± 2	118 ± 4	114 ± 8
σ_{UTS}, MPa	323 ± 4	417 ± 2	395 ± 6	373 ± 20	347 ± 24
$\sigma^{true}_{fracture}$, MPa	463 ± 4	645 ± 1	627 ± 26	634 ± 60	572 ± 48
$\varepsilon_{failure}$	0.43 ± 0.02	0.47 ± 0.07	0.49 ± 0.02	0.55 ± 0.04	0.53 ± 0.04
K (0.01–0.1), MPa	650 ± 16	572 ± 2	511 ± 48	408 ± 20	325 ± 18
n (0.01–0.1)	0.16 ± 0.01	0.12 ± 0.01	0.13 ± 0.02	0.11 ± 0.01	0.09 ± 0.02
K (0.1–0.15), MPa	739 ± 8	922 ± 2	898 ± 34	731 ± 48	680 ± 18
n (0.1–0.15)	0.18 ± 0.02	0.20 ± 0.01	0.23 ± 0.01	0.21 ± 0.02	0.21 ± 0.02

and an artificial human sweat solution. The results of the FCP testing are given in Table 4. For the Na_2SO_4 solution, the C77D, C99H, and C99R are more cathodic (negative) compared to the commercial alloys C77000 and C73100 alloys. The C99R has the lowest FCP after 6000 s. The FCP of C71300 binary alloy fluctuated more than the C77000 and the C77D alloys and did not reach an apparent steady-state potential after a 24-h exposure. The behavior of the binary alloy was also substantially more anodic (positive) than the other alloys. This behavior of the C71300 alloy in the Na_2SO_4 suggests that active corrosion may be occurring, as this would tend to shift the potential toward that of the dominant reaction. Optical microscopy performed on the surfaces after the FCP test revealed significant evidence of both uniform corrosion and selective dissolution (dealloying) of the Zn in the Na_2SO_4 solution [12]. While Na_2SO_4 generally does not cause pitting, it can be a fairly aggressive environment for some Ni/Cu alloys. As such, some preferential attack of the Zn was expected after a 24-h exposure because the Zn activity is greater than that of Cu and Ni in this solution [36].

In the artificial human sweat solution, the prototype alloys also exhibit lower FCPs after 6000 s, with C99R having the lowest value (more cathodic) of the three prototypes. Surface examination of the C99R and C99H alloys revealed no indications of active corrosion. With respect to the behavior in the Na_2SO_4 solution, the FCP for the C71300 is more anodic compared to the other alloys, but the alloy does reach a steady-state potential in the sweat and did not indicate any active corrosion reactions. Compared to the optical microscopy results after the exposure to the Na_2SO_4, there was substantially less attack after the 24-h exposure in the artificial sweat. The attack on these surfaces was predominantly localized corrosion (pitting); however, small patches of uniform corrosion were also observed. No evidence of selective dissolution was apparent on these surfaces. Note that the composition of the simulated sweat solution is predominately distilled water with substantially less charge-carrying ions with respect to the sulfate solution, so the results may be more indicative of the lack of ionic species in this solution than an indication of the actual performance in service.

Figure 14 presents the polarization resistance as a function of the log current density for the design prototypes in the two solutions. In thermodynamic terms, the potential is the thermodynamic driving force for a particular corrosion reaction, and the current is the rate at which that reaction occurs. The current density (i.e., the current/surface area) is a normalized value that facilitates comparison between specimens. As shown in Fig. 14a, the behaviors of the three alloys were quite similar in the sulfate solution with the exception of the behavior of the C77000 binary being slightly more anodic at the minimum current. All three alloys exhibited a region with a relatively stable current density that suggests passivity in the sulfate solution, and the onset of pitting occurred at approximately 0.000 V with respect to Ag/AgCl for all three alloys. In general, the behaviors of the three alloys were fairly similar in the simulated sweat solution (Fig. 14b). Some differences were observed in the potential at minimum current values for the C77000 alloy; however, the anodic regions of the C71300, C77000, and C77D are remarkably similar. None of the alloys exhibited a region that suggests passivity in this environment and there was no clear indication that pitting occurred. Furthermore, the overall trend suggests that corrosion occurred almost immediately with an anodic current and continued in a uniform fashion until the maximum potential of the scan was reached. While the compositions of the simulated sweat solutions differed slightly, the overall trends for the C71300, C77000, and C77D are consistent with those reported in the literature [31, 32, 37]. As was noted earlier, these results may be more indicative of the lack of ionic species in this solution than an indication of the performance in service. As shown in Fig. 14c, the behaviors of the C99R and C99H are quite similar to C71300 in the sulfate solution. All three alloys exhibit a relatively stable passivity region in the sulfate solution. Like the behaviors C77000 and the C77D in Fig. 14a, the onset of pitting also occurred at approximately 0.000 V with respect to Ag/AgCl; however, pitting occurred at a higher current density for the C99H in comparison to the C71300

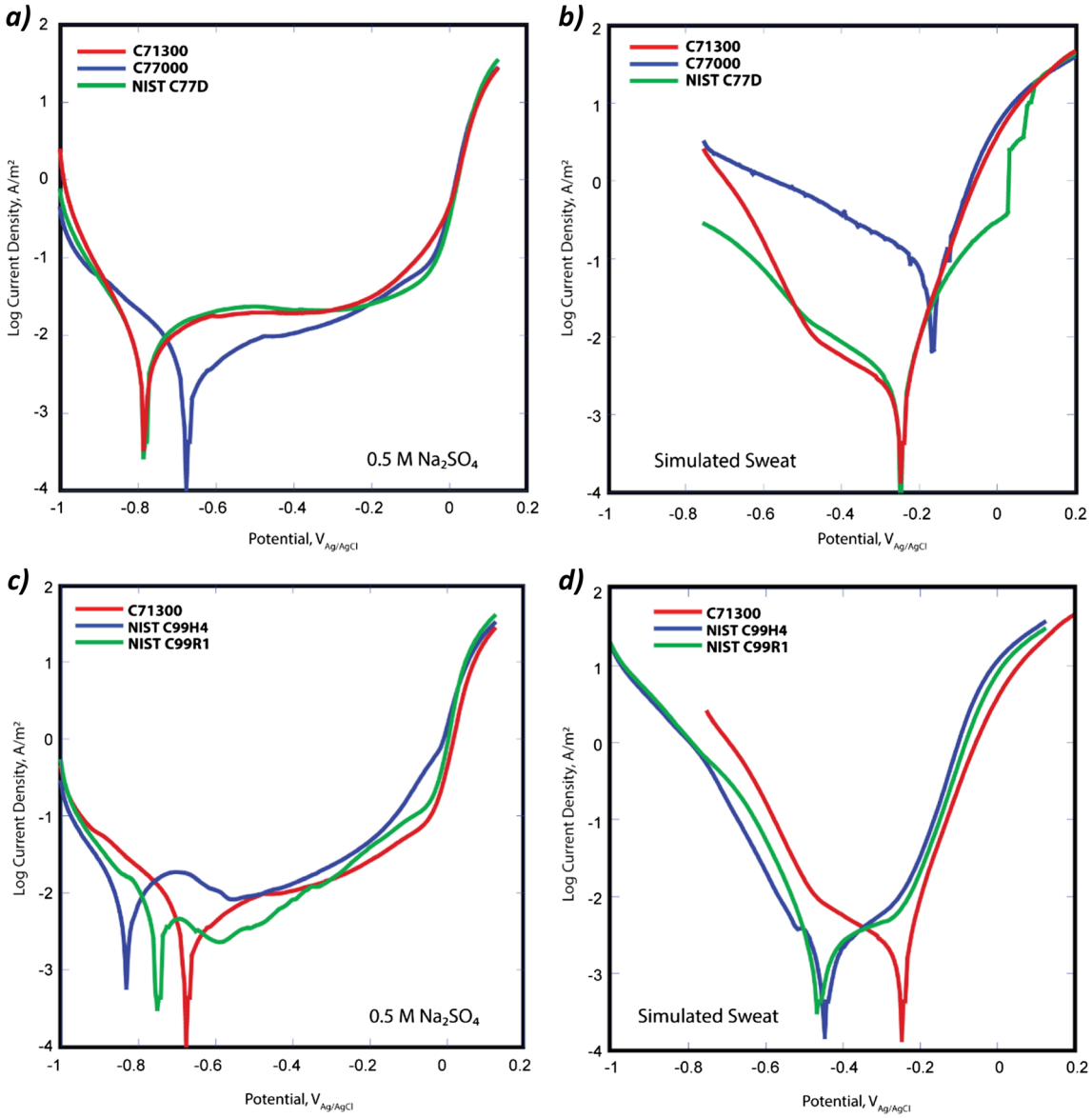

Fig. 14 Polarization resistance plots of the three NIST-designed alloys compared to commercial alloys C77000 and C71300 in deaerated 0.5 mol/L Na_2SO_4 solution, **a**, **c**, and deaerated simulated human sweat solutions, **b**, **d**

and the C99R. Overall, the behaviors of the C71300, C99H, and C99R were quite similar in the simulated sweat solution with the potential at minimum current being the only distinct difference between the three alloys. As was the case in Fig. 14b, none of the alloys exhibited a region that suggests passivity in this environment and there was no clear indication that pitting occurred.

Additional Prototype Characterization

Additional characterization was performed on the 2 kg rolled sheets of the three design prototypes by the US Mint. The US Mint successfully produced blanks and stamp coins using the rolled sheet of the design prototypes. Additional wear, corrosion, and vending machine testing of the prototype coins were completed. The results of wear and corrosion testing performed on C77D, C99R, and C71300 by the US Mint showed the C77D to exceed the performance to C71300. Details on the wear and corrosion testing performed by the US Mint are given in Stossel et al. [2].

Vending Machine Acceptance

Most vending machines use eddy current electrical conductivity measurement to identify the coins. Vending machines use a range of frequencies to make the identifications, so the acceptance of a coin can vary between individual machines. Those machines that use higher frequency ranges are sensitive to the

material at the surface of the coin, while those using lower frequency ranges tend measure the core material properties. The US Mint uses a variety of vending machine coin acceptors to evaluate the acceptance rate of coins for this reason. One hundred percent of the coins produced from the stamped prototype coin materials were accepted using the US Mint testing machines; however, the acceptance rate measured by a vendor external with a tighter acceptance window was 70%.

Composition Tolerances

Producing the desired 2 kg rolled sheet prototype materials for the US Mint required four heats of each prototype, and there was some unavoidable composition variation within the different heats. However, the composition variations provided valuable information for determining the composition tolerances for the prototype alloys. The composition variations from different heats also provided input on the acceptable impurity level for the prototypes. Iron is a known impurity in Cu introduced by recycled Cu. In general, Fe impacts the electrical conductivity behavior similarly to Mn, and as such, the Fe content is added to Mn content when modeling the electrical conductivity. As the electrical conductivity and color properties were most sensitive to small composition variations, the composition tolerances were determined by estimating the changes in these properties predicted by the CALPHAD-based models. Two alloys that represent the maximum and minimum of the C77D composition ranges were produced to verify predictions for the tolerances. The composition of these alloys and the measured electrical conductivities are given Table 6. The measured electrical conductivity confirmed the predictions of the composition tolerances. The lower and upper extrema for electrical conductivity were measured as (5.22 ± 0.07) % IACS and (5.75 ± 0.08) % IACS, respectively, confirming the calculated final alloy composition tolerances.

Currently, C99R is under investigation, designated as C99750T-M, as the most promising candidate for seamless replacement of C71300 in the production of US coinage, as mentioned in the US Mint 2016 Biennial Report to Congress regarding the "Coin Modernization, Oversight, and Continuity Act of 2010" (H.R. 6162), released in July of 2017.

Discussion/Conclusions

Lessons Learned During the Design Process

It was initially assumed that two separate design processes would be required to redesign the commercial C77000 to match the required electrical conductivity and to develop new low-cost monolithic alloys. Once the CALPHAD-based models were developed for the various material properties, it became clear that a continuum of alloys exists that all meet the initial design requirements, with the exception of color. For a desired electrical conductivity value, there is a clear trade-off between the cost and color. The cost is decreased by reducing the amount of Ni. However, as the Ni content is decreased, the amount of Mn needed to maintain the desired electrical conductivity increases and the color of the alloy becomes less desirable (more yellow). C99R represents the best possible (i.e., lowest cost) alloy that meets the subjectively designated esthetic acceptability [13, 38]. Further cost savings are possible if an increased degree of "yellowness" is accepted. As such, C99G is one of the most cost-effective alloys possible within these design parameters. Therefore, if cost reduction is the principal driver for new coinage alloys, it may be possible to achieve additional reductions in materials cost in the future by relaxing the esthetic color restraint.

Table 6 Alloy produced to identify the upper and lower composition tolerances of the NIST designed C77D prototype alloy

Alloy	C77G (lower σ-limit)	G77H (upper σ-limit)
Cu, %	Bal.	Bal.
Ni, %	20 (20.07 ± 0.36)	18 (18.19 ± 0.68)
Zn, %	24 (23.64 ± 0.46)	28 (27.59 ± 0.48)
Mn, %	0.5 (0.45 ± 0.06)	0.2 (0.20 ± 0.08)
Fe, %	0.2 (0.16 ± 0.08)	N/A
σ, %IACS	5.22 ± 0.07	5.75 ± 0.08

The compositions in parentheses are the experimentally measured values, which differ slightly from the nominal

Conclusions

Three new coinage alloys were designed using systems design approach and CALPHAD-based models for the thermodynamics, electrical conductivity, color, and cost. The CALPHAD models were focused on the Cu-Ni-Zn-Mn system. The CALPHAD-based electrical conductivity model was constructed based on available data from the literature for the unary, binary, and a limited number of commercial alloys. Additional alloys were developed to determine missing binary parameters and to validate ternary and quaternary descriptions. A basic composition-dependent color model was developed for the Cu-Ni-Zn-Mn system using the work of Lahiri. Characterization of the three designed prototypes confirmed that each of the prototypes were able to achieve the design objectives. The systems design approach highlighted the trade-offs between reducing the cost of the alloy and achieving the desired color objectives. Lower cost alloys could be developed using this computational approach, if the color restraints were relaxed. The current design was restricted to current processing capabilities; however, if additional

processing capabilities were available, such as expanding the annealing temperature range or variations in the quenching rates, wider composition ranges might be accessible for the design.

Acknowledgments Funding for this work was provided by an Interagency Agreement between the United States Mint and the National Institute of Standards and Technology, HQ14RA-38 NISTMOD. 001 (IA# 1404-642-01). The authors gratefully acknowledge Tony Ying of the United State Mint for providing stamping, vending machine testing, and additional color and electrical conductivity measurements.

References

1. "COIN MODERNIZATION, OVERSIGHT, AND CONTINUITY ACT OF 2010," Public Law 111-302, 31 U.S.C. 5112 Chapter 51, Congressional Record, 2010
2. R.J. Stossel, M.L. Tims, J.R. Pickens, D.K. McNamara, M.G. McCann, R.F. Decker, Alternative metal study; August 31, 2012
3. Olson GB (2013) Genomic materials design: ihe ferrous frontier. Acta Mater 61:771–781
4. Olson GB (1997) Computational design of hierarchically structured materials. Science 277:1237–1242
5. Cohen M (1976)Unknowables in the essence of materials science and engineering. Mater Sci Eng 25:3–4
6. C.S. Smith (1981) A search for structure. MIT Press
7. H.J. Wagner, A.M. Hall (1966) The New Coinage. J Metals 18: 300–307
8. Kimber RA, Stokes RR (1966) Bell Syst Tech J XVL:30
9. Schweckandt DS, Aguirre MdC (2015) Electrodeposition of Ni-Co alloys. determination of properties to be used as coins. Proc Mater Sci 8:91–100
10. Song JY, Hong SI (2011) Design and characterization of new Cu alloys to substitute Cu–25%Ni for coinage applications. Mater Des 32:1790–1795
11. J.F. Breedis, D.E. Trumbull (1995) Copper alloy clad for coinage, United States Patent Office, 5,472,796
12. B.P. Oberursel, M.B.R. Friedrichsdorf, G.R. Neuberg, U.H. Werdohl, H.Z. Altena (1983) Gold-colored coin material, United States Patent Office, 4,401,488
13. E.A. Lass, M.R. Stoudt, T. Ying, C.E. Campbell, Alloy development and characterization services for United States currency applications, NIST, Gaithersburg, MD, 2015, Internal Report 1404–642-01
14. E.A. Lass, M.R. Stoudt, T. Ying, C.E. Campbell (2015) Systems design approach to low-cost coinage materials data, http://hdl.handle.net/11256/961
15. Thermo-Calc Software (2015b) Thermo-Calc AB, Stockholm, Sweden 2015
16. Solid Solution Database (2010), Scientific Group Thermodata Europe (SGTE)
17. M.A. Dayananda, C.L. Liu (1990) Fundamentals and applications of ternary diffusion. Proc Int Symp Hamilton Ont 91–100
18. Rooy AD, Bronsveld PM, De Hosson JTM (1982) Z Met 73:610–615
19. Jiang M, Wang CP, Liu XJ, Ohnuma I, Kainuma R, Vassilev GP, Ishida K (2005) Thermodynamic calculation of phase equilibria in the Cu–Ni–Zn system. J Phys Chem Solids 66:246–250
20. Miettinen J (2003) Thermodynamic description of the Cu–Ni–Zn system above 600◦C. CALPHAD 27:263–274
21. Miettinen J (2003) Thermodynamic description of the Cu–Mn–Ni system at the Cu–Ni side. CALPHAD 27:147–152
22. Miettinen J (2004) Thermodynamic description of the Cu–Mn–Zn system in the copper-rich corner. CALPHAD 28:313–320
23. Campbell CE, Kattner UR, Liu ZK (2014) Integr Mater Manuf Innov 3:23
24. Nordheim L (1931) Ann Phys-Berlin 9:607–640
25. Terada Y, Ohkubo K, Mohri T, Suzuki T (2000) Mater Sci Eng A 278:292–294
26. K. Schroder (1983) CRC handbook of electrical resistivitives of binary metallic alloys
27. Lahiri A, Mukherjee K, Banerjee T (1966) Symposium on metallurgy of substitute ferrous & non-ferrous alloys. NML, Jamshedpur
28. R.M. German, M.M. Guzowski, W.D. C (1980) Color and color stability as alloy design criteria. J Metals 32(3):20–27
29. Fredj N, Kolar JS, Prichard DM, Burleigh TD (2013) Study of relative color stability and corrosion resistance of commercial copper alloys exposed to hand contact and synthetic hand sweat. Corros Sci 76:415–423
30. Liang C-h, Wang S-s, Huang N-b, Wang P (2015) Corrosion behavior of brass coinage in synthetic sweat solution. Trans Nonferrous Metals Soc China 25:654–660
31. Milošev I, Kosec T (2007) Study of Cu–18Ni–20Zn nickel silver and other Cu-based alloys in artificial sweat and physiological solution. Electrochim Acta 52:6799–6810
32. Porcayo-Calderon J, Rodríguez-Díaz RA, Porcayo-Palafox E, Martinez-Gomez L (2016) Corrosion performance of Cu-based coins in artificial sweat. J Chem 2016:1–11
33. E.A. Lass, M.R. Stoudt, C.E. Campbell, T. Ying (2018) Alloy with selected electrical conductivity and atomic disorder, process for making and using same, April 19, United States Patent Office, 9,951,406
34. E.A. Lass, M.R. Stoudt, C.E. Campbell, T. Ying Coinage cladding alloy and processing for making coinage cladding alloy, United States Patent application 201801059 accepted April 19, 2018
35. E.A. Lass, M.R. Stoudt, C.E. Campbell, T. Ying Coinage alloy and processing for making coinage alloy, United States Patent application 20180105911, accepted April 19, 2018
36. Jones DA (1992) Principles and prevention of corrosion. Macmillan Publishing Co, New York, NY
37. Zhou X-Z, Deng C-P, Su Y-C, Alloy J (2010) Comparative study on the electrochemical performance of the Cu–30Ni and Cu–20Zn–10Ni alloys. Compounds 491:92–97
38. E.A. Lass, M.R. Stoudt, C.E. Campbell, T. Ying; Coinage alloy and processing for Making coinage alloy, United States Patent application 20180105912, accepted April 19, 2018